Remote Sensing of Environment 238 (2020) 111018

Contents lists available at ScienceDirect

Remote Sensing of Environment

journal homepage: www.elsevier.com/locate/rse

Investigating impacts of drought and disturbance on evapotranspiration over a forested landscape in North Carolina, USA using high spatiotemporal resolution remotely sensed data

Yun Yang[a,*], Martha Anderson[a], Feng Gao[a], Christopher Hain[b], Asko Noormets[c], Ge Sun[d], Randolph Wynne[e], Valerie Thomas[e], Liang Sun[a]

[a] USDA ARS, Hydrology and Remote Sensing Laboratory, Beltsville, MD, United States of America
[b] Marshall Space Flight Center, Earth Science Office, Huntsville, AL, United States of America
[c] Department of Ecosystem Science and Management, Texas A&M University, TX, United States of America
[d] USDA Forest Service Southern Research Station, Research Triangle Park, NC, United States of America
[e] Department of Forest Resources and Environmental Conservation, Virginia Polytechnic Institute and State University, VA, United States of America

ARTICLE INFO

Keywords:
Evapotranspiration (ET)
Drought
Disturbance
Forest
Landsat
Time series
Data fusion

ABSTRACT

Forest ecosystem services such as clean water, wildlife habitat, and timber supplies are increasingly threatened by drought and disturbances (e.g., harvesting, fires and conversion to other uses), which can have great impacts on stand development and water balance. Improved understanding of the hydrologic response of forested systems to drought and disturbance at spatiotemporal resolutions commensurate with these impacts is important for effective forest management. Evapotranspiration (ET) is a key hydrologic variable in assessing forest functioning and health, but it remains a challenge to accurately quantify ET at landscape scales with the spatial and temporal detail required for effective decision-making. In this study, we apply a multi-sensor satellite data fusion approach to study the response of forest ET to drought and disturbance over a 7-year period. This approach combines Landsat and Moderate Resolution Imaging Spectroradiometer (MODIS) ET product time series retrieved using a surface energy balance model to generate a multi-year ET datacube at 30-m resolution and daily timesteps. The study area (~900 km^2) contains natural and managed forest as well as croplands in the humid lower coastal plains in North Carolina, USA, and the simulation period from 2006 to 2012 includes both normal and severe drought conditions. The model results were evaluated at two AmeriFlux sites (US-NC2 and US-NC1) dominated by a mature and a recently clearcut pine plantation, respectively, and showed good agreement with observed fluxes, with 8–13% relative errors at monthly timesteps. Changes in water use patterns in response to drought and disturbance as well as forest stand aging were assessed using the remotely sensed time series describing total evapotranspiration, the transpiration (T) component of ET, and a moisture stress metric given by the actual-to-reference ET ratio (f_{RET}). Analyses demonstrate differential response to drought by land cover type and stand age, with larger impacts on total ET observed in young pine stands than in mature stands which have substantially deeper rooting systems. Transpiration flux shows a clear ascending trend with the growth of young pine plantations, while stand thinning within the plantation leads to decreases in both remotely sensed leaf area index and T, as expected. Time series maps of f_{RET} anomalies at 30-m resolution capture signals of drought, disturbance and the subsequent recovery after clearcut at the stand scale and may be an effective indicator for water use change detection and monitoring in forested landscapes.

1. Introduction

Forests provide many important ecosystem service functions, including wildlife habitat, timber production and watershed water regulation (Sun et al., 2017b). Decline in forests can be caused by many factors, generally relating to human or nature-induced disturbance and changing climate. In this context, disturbance includes forest harvesting, thinning, wind throw, fire, ice storm, landslide, flooding, avalanche, insect outbreaks, and land conversion. Changes in climate, including air temperature, humidity and precipitation regime, also

* Corresponding author at: 10300 Baltimore Ave, Beltsville, MD 20705, United States of America.
E-mail address: yun.yang@ars.usda.gov (Y. Yang).

https://doi.org/10.1016/j.rse.2018.12.017
Received 22 December 2017; Received in revised form 8 December 2018; Accepted 10 December 2018
Available online 21 December 2018

affect forest ecosystems and can serve as a modulator of disturbances. For example, short-term drought can make forests more susceptible to insect attack and wildfire, while prolonged drought can directly cause tree mortality (Allen et al., 2010; Anderegg et al., 2015). To better understand the influence of disturbance and drought on forests, numerous studies have been conducted using field observations collected under natural conditions (Anderegg et al., 2012, 2015; Baldocchi, 1997; Clinton et al., 1997; Noormets et al., 2010; Sun et al., 2015) and under simulated drought such as via throughfall reduction (Anderegg et al., 2013; MacKay et al., 2012; Wullschleger and Hanson, 2006). In these studies, the focus has generally been on observing the response of individual trees/stands over limited time periods. Given that trees with different ages, species and underlying edaphic conditions may respond differently to climate drivers (Esper et al., 2008; Yang et al., 2017b), conclusions drawn from data collected for individual trees may be modified at the forest stand or watershed level (Clark et al., 2016).

To complement in situ measurements, remote sensing data have been adapted for forest ecosystem research, exploiting the broad coverage and long-time series of measurements provided by the collective suite of available Earth observing systems. Many studies have used Moderate Resolution Imaging Spectroradiometer (MODIS) vegetation index data to monitor forest condition around the world at scales of 250 m and coarser (Saleska et al., 2007; Sims et al., 2006; Verbesselt et al., 2009). At finer scales, Landsat data at 30 m resolution have been used to monitor forest disturbance through resulting changes in surface reflectance (Masek et al., 2008; Wulder et al., 2008; Huang et al., 2010; Zhu et al., 2012; Kennedy et al., 2014; Cohen et al., 2016; Wang et al., 2016; Zhu, 2017). While these studies focused more on mapping disturbance and recovery and analyzing causality agents, relatively few studies have looked at the impact of disturbance and drought on water and energy balance within forest landscapes, especially at spatial and temporal scales capable of resolving variability in impacts. These balances can be effective indicators of ecosystem health and functioning and impact on water yield (Boggs et al., 2015; Cornish and Vertessy, 2001).

Evapotranspiration (ET) is a key component of both water and energy budgets. ET links the biological and hydrological cycles, and it is a critical variable in many physical-based eco-hydrological models (Sun et al., 2011a, 2011b, 2016). To assess the impact of disturbance and drought on water use in forested systems, three generalized methods of ET estimation have typically been employed (Domec et al., 2012; Sun et al., 2016). High temporal resolution measurements of ET have been made worldwide using eddy covariance (Baldocchi, 1997) and sapflow techniques (Kume et al., 2007; MacKay et al., 2012; Oishi et al., 2008). For watershed scale ET estimates, water balance methods have been used to calculate ET as the residual of precipitation and runoff (Vose and Swank, 1994; Sun et al., 2010); however, the underlying assumption that change in soil water storage is zero may not be appropriate for estimating ET at daily time steps. A third approach uses hydrologic models to estimate ET (Domec et al., 2015; Sun et al., 2011b), accounting for the full watershed hydrological cycle. Recently, remote sensing has been accepted by the forest community as a means to estimate stand-level ET, providing information about the spatial dynamics of water use at large scales (Sun et al., 2011b, 2016), which is not possible from traditional observation methods.

One common remote sensing method for estimating ET is the surface energy balance approach based on land surface temperature (LST) retrieved from thermal infrared (TIR) imagery. LST is an effective diagnostic indicator of the land surface moisture status (Anderson et al., 2011, 2012a; Karnieli et al., 2010; Sandholt et al., 2002). One challenge of using remotely sensed LST is the limited availability of high spatiotemporal resolution observations. MODIS provides near daily LST observations but only at 1 km spatial resolution. Landsat has higher spatial resolution (60–120 m), but the revisit time is 16 days for a single platform, and clear-sky acquisitions can be much less frequent in areas with persistent cloud cover. To address this issue, data fusion techniques have been used to combine MODIS and Landsat ET time series to generate daily ET maps at Landsat spatial resolution. ET fusion analyses using the Spatial and Temporal Adaptive Reflectance Fusion Model (STARFM; Gao et al., 2006) have been successfully applied over rainfed and irrigated crops (Cammalleri et al., 2013, 2014; Sun et al., 2017a, 2017b, 2017c; Yang et al., 2017a) and irrigated vineyards (Semmens et al., 2016) to study variability in water use patterns over agricultural landscapes. Yang et al. (2017b) described the first application of this system to a forested landscape, evaluating model performance at Landsat scale for a clearcut and a mature pine plantation site in North Carolina, USA for a single growing season during 2013.

In this paper, we expand on the investigation of Yang et al. (2017b), using a multi-year time series of 30-m daily ET data from the fusion methodology to investigate changes and trends in water use in the North Carolina study site over multiple growing seasons, covering the period 2006 to 2012. This period includes two consecutive years of severe drought – 2007 and 2008 – as well as forest thinning in 2009 (Liu et al., 2018). The Landsat 30-m resolution provided by the data fusion system enables evaluation of ET response at the scale of land management, facilitating investigation of coupling between land and water use change. The objectives of this study were: (1) to evaluate the accuracy of multi-year ET retrieval in comparison with eddy flux tower observations in young and mature managed forest stands, respectively; (2) to assess the drought impact on ET over different land cover types and pine plantations with various stand ages; (3) to assess the impact of disturbance on pine stand ET and the subsequent recovery in consumptive water use.

2. Methods

The multiscale ET framework used in this study includes the regional scale Atmosphere-Land Exchange Inverse (ALEXI) model based on thermal data from geostationary satellites (4-km resolution) and an associated disaggregation algorithm (DisALEXI) that uses higher resolution MODIS (1 km) and Landsat (60–120 m) thermal infrared imagery to downscale ALEXI fluxes. The MODIS and Landsat retrieved ET are subsequently fused to generate high spatiotemporal resolution ET time series using Spatial and Temporal Adaptive Reflectance Fusion Model (STARFM). A summary of this multiscale ET system is provided below; additional details regarding the ET fusion process can be found in Cammalleri et al. (2013, 2014) and other papers cited below.

2.1. ALEXI/DisALEXI

The foundation of ALEXI and DisALEXI is the two source energy balance (TSEB) model, which was developed by Norman et al. (1995) and further refined by Kustas and Norman (1996). The TSEB model partitions the observed directional radiometric surface temperature and derived energy fluxes between two nominal sources: the soil and vegetation components of the scene (Eqs. (1) and (2))

$$R_{n,s} = H_S + LE_S + G_0 \quad (1)$$

$$R_{n,c} = H_c + LE_c \quad (2)$$

where the subscripts “s” and “c” represent soil and canopy energy flux components (in W m^{-2}), R_n is net radiation, H is sensible heat flux, LE is latent heat flux and G_0 is soil heat flux. Directional surface radiometric temperature ($T_{RAD}(\varnothing)$) partitioning is approximated using the local fraction of vegetation cover, $f(\varnothing)$, observed at the view angle ($\varnothing$) of the thermal sensor:

$$T_{RAD}(\varnothing)^4 = f(\varnothing)T_c^4 + [1 - f(\varnothing)]T_s^4 \quad (3)$$

where $f(\varnothing)$is derived from a remotely sensed leaf area index (LAI) estimate using Beer's Law. The diagnosed soil and canopy temperatures, T_s and T_c, are used to constrain the sensible heat fluxes H_s and H_c using a series resistance formalism coupling the two sources with the in-

canopy and above-canopy air temperature (Kustas and Norman, 1999, 2000). Canopy transpiration (LE_c) is estimated with a modified Priestley-Taylor approach with the initial assumption that the vegetation is under unstressed conditions, and soil evaporation (LE_s) computed as a residual to the soil energy budget. If LE_s is less than zero, LE_c is down-regulated from the unstressed rate, governed by the assumption that condensation onto the soil ($LE_s < 0$) under daytime clear-sky conditions is unlikely. Further information regarding the TSEB model is provided by Kustas and Anderson (2009).

The regional scale ALEXI model applies the TSEB to observations of morning LST rise acquired from geostationary platforms (Anderson et al., 1997, 2007). Instead of using absolute instantaneous LST measurements, a time-differential measurement is used to reduce impact of biases incurred in the calibration and atmospheric correction of the LST retrievals. ALEXI combines TSEB with a simple slab model of morning atmospheric boundary layer (ABL) growth to obtain energy closure over this morning time period. To produce ET estimates at higher resolution than can be supported from geostationary data, the ALEXI fluxes can be spatially disaggregated with the DisALEXI approach (Anderson et al., 2004; Norman et al., 2003) using finer scale air- or spaceborne remote sensing observations. Further information about ALEXI/DisALEXI can be found in Anderson et al. (2005, 2008, 2010, 2012b).

2.2. Data fusion

In this study, MODIS and Landsat derived variables (LST, LAI, and surface albedo) were used as input to DisALEXI to obtain 1-km MODIS scale (near daily) and 30-m Landsat scale (periodic) ET retrievals. Prior to fusion, gaps in Landsat scene coverage resulting from cloud cover or the scan line corrector failure on Landsat 7 are filled using the gap-filling procedure described in Yang et al. (2017b). MODIS ET maps are gap-filled to daily coverage by temporally interpolating the ratio of MODIS to ALEXI ET determined for clear pixels in the MODIS time series.

Gap-filled ET retrievals from DisALEXI using MODIS and Landsat TIR data are then fused to generate daily Landsat-scale ET time series using STARFM (Gao et al., 2006). STARFM uses MODIS-Landsat image pairs available on clear Landsat overpass dates to predict Landsat-scale images on MODIS dates between Landsat overpasses. While the algorithm was originally designed to fuse surface reflectance imagery (Gao et al., 2015, 2017), STARFM has also been successfully applied to Landsat and MODIS ET products as well (Anderson et al., 2018; Cammalleri et al., 2013, 2014; Semmens et al., 2016; Sun et al., 2017a, 2017b, 2017c; Yang et al., 2017a, 2017b, 2018). In this case, the MODIS ET time series effectively conveys information about changes in surface moisture status and consumptive water use that occur at the 1 km scale or larger and between Landsat dates.

2.3. Fraction of reference ET time series and anomalies

In addition to looking at the dynamics of actual ET in this forested landscape, we also investigate the behavior of a normalized ET metric, f_{RET} - defined as the ratio between actual ET and a reference ET describing an upper limit on ET expected under well-watered conditions. Here we use a grass reference ET calculated using the Food and Agriculture Organization (FAO) Penman-Monteith method (Allen et al., 1998). Normalization by reference ET reduces response to variations in insolation and atmospheric demand, focusing the f_{RET} metric more on the impact of soil moisture limitations. Standardized anomalies in f_{RET} compared to baseline conditions computed on average over multiple years are used to produce the Evaporative Stress Index (ESI), proposed by Anderson et al. (2007) as a new ET-based remote sensing drought indicator. The ESI at 4-km spatial resolution has demonstrated capabilities for early warning of stress onset during flash drought (Anderson et al., 2013, 2016; Otkin et al., 2013, 2016). While standardized anomalies in f_{RET} can be computed for long time series (e.g. longer than 10 years), here we look at the anomaly of f_{RET} (Δf_{RET}), which may be more appropriate for shorter study periods where the standard deviations cannot be reliably determined. Here, Δf_{RET} has been computed as:

$$\Delta f_{RET}(d, y_k, i, j) = f_{RET}(d, y_k, i, j) - \frac{1}{n}\sum_{k=1}^{k=n} f_{RET}(d, y_k, i, j) \quad (4)$$

where $f_{RET}(d, y_k, i, j)$ is the value of f_{RET} for day d, year y_k, and i, j grid location, and n is the number of all years in the period of record. In this study, we examine f_{RET} and Δf_{RET} at Landsat resolution - at the patch/plot scale where we can resolve stress behavior of fields with different land cover types, stand ages and management strategies.

2.4. Statistical analysis

Model performance is assessed through statistical comparison of observations collected at flux tower sites with time series of modeled ET and other flux components extracted over the tower footprint sampling area. Statistical metrics of performance including mean bias error (MBE), root mean square error (RMSE), mean absolute error (MAE), and relative error (RE) defined as the ratio of MAE and the mean observed flux (Ô), were calculated using the observed and simulated ET on Landsat overpass dates, and on daily and monthly timesteps using model estimates from the fused, time-continuous ET datacube.

In addition, trends in forest recovery after disturbance were analyzed using simple linear trend methods, reporting the coefficient of determination (R^2), MAE and RMSE of the linear regression.

3. Study site and datasets

3.1. Study domain

The study area is located on the lower coastal plain of North Carolina (Fig. 1). The climate type is classified as outer coastal plain mixed forest province (Bailey, 1995). The long-term (1945–2014) average annual precipitation is 1321 mm, with rainfall evenly distributed throughout the year. The long-term average annual temperature is 15.5 °C, with monthly temperature ranging from 26.6 °C in July to 6.4 °C in January. The Parker Tract research site was established in the early 1990s in loblolly pine (*Pinus taeda*) plantations that are maintained for timber production and commercially managed by the Weyerhaeuser Company (Domec et al., 2012; Liu et al., 2018; Noormets et al., 2010; Sun et al., 2010). The USDA Forest Service maintains this long-term research site to study forest hydrology and carbon flux under conditions of intensive management. The study area includes wetlands that were drained using parallel ditches to improve timber production in the lower coastal plains (Domec et al., 2012). Other major land cover types include wetland, hardwood natural forest and crop land.

The simulation period covered the years 2006–2012, and included a multi-year drought event that impacted the study domain from the summer of 2007 through 2008. The annual precipitation for 2007 and 2008 as measured on site was 899 mm and 822 mm, respectively (Fig. 2) - > 400 mm below the long-term average for the region. Year 2011 also had a dry growing season, although the annual precipitation for 2011 was normal.

3.2. Flux sites

The US-NC1 flux site (35°48′N, 76°42′W) was installed in 2005 to study carbon and water fluxes in a young loblolly pine plantation. The 70-ha study site was originally a native hardwood forest and was harvested via clearcut in 2002. In 2004, 2-year old loblolly pine seedlings were planted at a 1.5-m by 6-m spacing (Sun et al., 2010). The soil in the US-NC1 site is a dark sandy loam in the top 25 cm, sandy clay loam at the depth of 25–69 cm, sandy loam at the depth of 60–75 cm, and

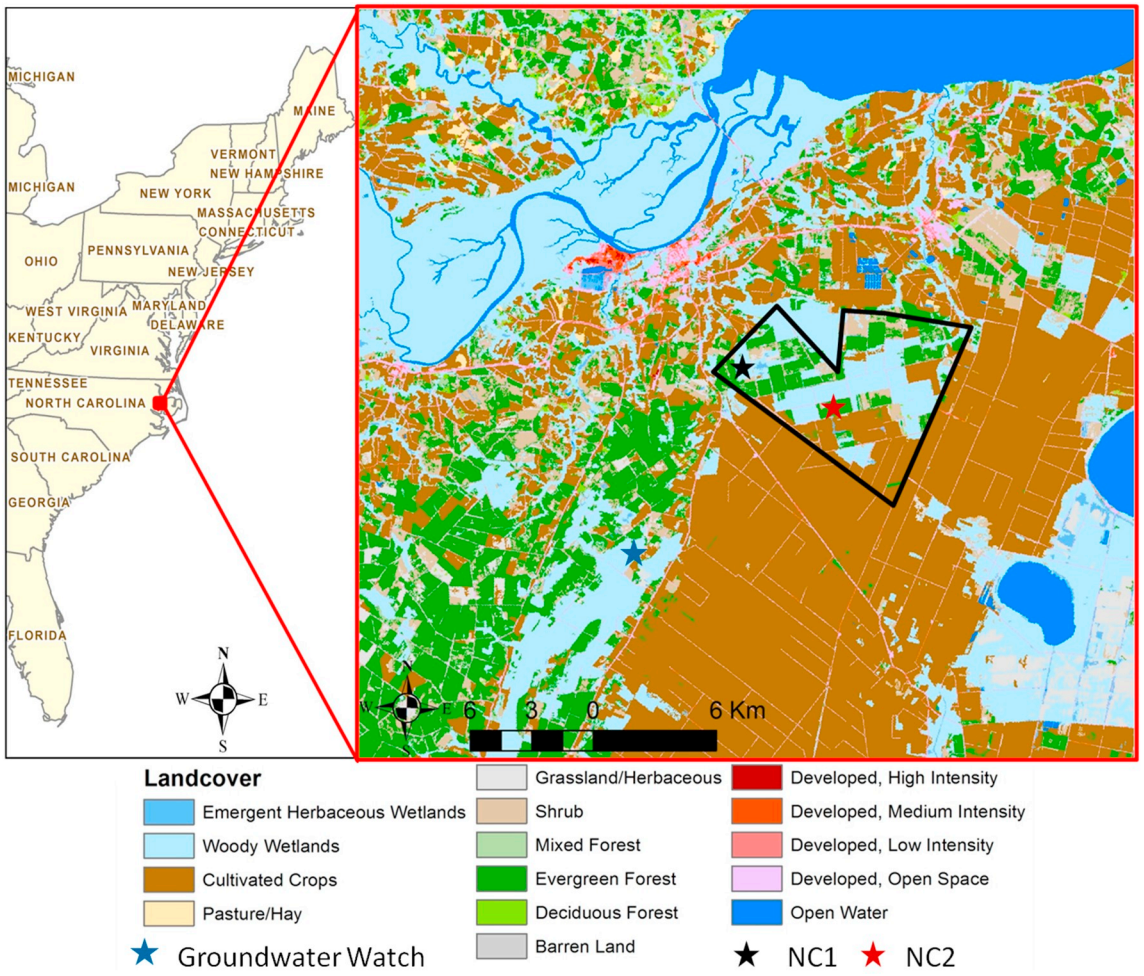

Fig. 1. Land cover types over the study area as defined by the 2006 National Land Cover Dataset (NLCD). The area within black outline is the pine plantation. The black and red stars indicate the Ameriflux NC1 and NC2 flux tower locations, and the blue star is the location of a USGS groundwater station. (For interpretation of the references to color in this figure legend, the reader is referred to the web version of this article.)

gray sandy clay at the depth of 75–155 cm (Diggs, 2004).

The US-NC2 (35°48′N, 76°40′W) tower is in a mid-rotation plantation stand with 90 ha area, which was established after clearcutting a previous rotation of loblolly pine, replanted with 2-year old seedlings at 1.5 m by 4.5 m spacing in 1992. The soil type in the study area is Belhaven series Histosol, which is mainly coarse glacial outwash sand covered by a 50–85 cm depth organic layer (Sun et al., 2010). The stand has been fertilized twice – at establishment, and in 2010 following a

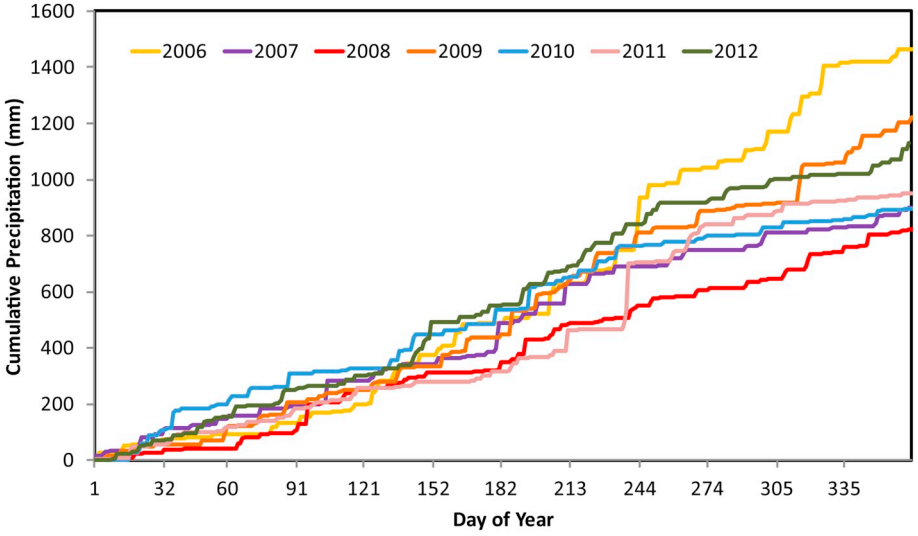

Fig. 2. Annual cumulative measured daily precipitation for the period from 2006 to 2012 at the NC1 flux tower site.

thinning in late 2009. The thinning event removed trees from every fourth row and selectively thinning from the remaining rows, which removed approximately 50% of the basal area (Gavazzi et al., 2016; Liu et al., 2018). The understory was composed of red maple, greenbrier and volunteer loblolly pine.

3.3. Model input data

The main remote sensing inputs for the multiscale ET mapping system include LST, LAI, and albedo, which are developed at regional scale for ALEXI and at finer scale (MODIS and Landsat) for DisALEXI. Meteorological data used for both ALEXI and DisALEXI were obtained from the Climate Forecast System Reanalysis (CFSR) dataset from the National Centers for Environmental Prediction (NCEP) (Saha et al., 2010). All input data were resampled to 4-km for ALEXI, to 1-km (MODIS) and 30-m (Landsat) for DisALEXI.

3.3.1. ALEXI

The ALEXI model has been run daily on a 4-km resolution grid over the continental U.S. since 2001 using LST inputs obtained from the Geostationary Operational Environmental Satellite (GOES) East and West imager instruments. Daily LAI inputs to ALEXI data are aggregated and temporally interpolated from the 1-km 4-day MODIS LAI (MCD15A3) product, while albedo is derived from soil and canopy reflectances trained on MODIS albedo products. Further details about the ALEXI process are provided by Anderson et al. (2007, 2012b).

3.3.2. DisALEXI-MODIS

MODIS disaggregation of the 4 km ALEXI data used instantaneous 1-km swath LST data (MOD11_L2, (Wan et al., 2004)), which were converted to geographic coordinates with the MODIS Reprojection Tool (MRT) using associated geolocation data (MOD03). LAI data were obtained from the 4-day MCD15A3 (Myneni et al., 2002) product, and converted to geographic coordinates with MRT. Albedo inputs were from the 8-day MCD43GF (Sun et al., 2017a, 2017b, 2017c) global product at 1-km spatial resolution in geographic coordinates. All data were from MODIS collection 5 and went through quality check using the associated data quality band, retaining only data classified as having good quality. For MODIS LST, we extracted the mandatory QA, data quality, and cloud flags, and retained data deemed cloud free and of good quality based on these flags. For MODIS LAI data, both FparLai_QC and FparExtra_QC layers were used to screen out significant or mixed clouds, internal clouds, cloud shadow, snow, dead detectors or invalid LAI values. For MODIS albedo, the high quality full inversion values were extracted based on the associated QA map.

3.3.3. DisALEXI-Landsat

Landsat disaggregation of the 4 km ALEXI data was performed on a 30-m resolution UTM grid associated with the Landsat Worldwide Reference System (WRS)-2, using thermal infrared (TIR) and shortwave surface reflectance data from Landsats 5 and 7. The TIR data were downloaded from USGS EarthExplorer and atmospherically corrected using MODTRAN (Cook et al., 2014), while atmospherically corrected surface reflectance data were ordered and downloaded from USGS ESPA. Pixels indicated as cloud and cloud shadow in the pixel quality band were screened out. Eighty images (path 14/row 35) with less than ~75% cloud coverage were used in this study (Fig. 3). Atmospherically corrected Landsat TIR imagery was sharpened from its native spatial resolution (120 m for Landsat 5 and 60 m for Landsat 7) to 30 m with a Data Mining Sharpening (DMS) method using multi-band surface reflectance maps (Gao et al., 2012b). Landsat-scale LAI was generated with a regression tree approach that effectively downscales MODIS LAI products using Landsat shortwave surface reflectance data (Gao et al., 2012a). This MODIS-based LAI approach is used to maximize Landsat-MODIS ET compatibility, improving the fusibility of these two image time series.

3.3.4. Biophysical data

A stand age map developed by Weyerhaeuser Company in 2013 provides planting information for each stand. When extracting data from the gridded model output based on stand age, a 60-m buffer inside the edge of each plot was applied to avoid pixels mixed with roads or other stands. Land cover information at 30-m resolution was obtained from the 2006 National Land Cover Dataset (NLCD) (Fry et al., 2011) (Fig. 1), and was used in Landsat disaggregation. For MODIS disaggregation, these data were aggregated to 1-km based on dominant cover type. Land cover type is used in ALEXI/DisALEXI to set pixel-based vegetation parameters (e.g. leaf reflectance in the visible, NIR and TIR bands) and to define roughness parameters related to canopy height, following Cammalleri et al. (2013). Many plots within the Parker Tract plantation, including NC1 and NC2, are erroneously classified as woody wetland by NLCD 2006 (see Fig. 1); however, these stands are treated as evergreen forest in this study.

3.3.5. Micrometeorological data

Energy fluxes at both NC1 and NC2 were measured using an open-path eddy covariance system, which includes a CSAT3 three-dimensional sonic anemometer (Campbell Scientific Instrument-CSI, Logan, UT, USA[1]), a CR5000 data logger (CSI), an infrared gas analyzer (IRGA, Model LI-7500, LI-COR, Lincoln, NE, USA) and a relative humidity and air temperature sensor (model HMP-45C; Vaisala Oyj, Helsinki, Finland) (Noormets et al., 2010; Sun et al., 2010; Liu et al., 2018). Soil heat flux was measured at NC2 with three heat flux plates (model HFT3, CSI, Logan, UT, USA) at the depth of 2 cm. The soil heat flux plates were placed in three contrasting microsites - one in a row of trees in relative shade, another between rows in a mostly open environment, and one about half-way in between. Net radiation was measured with 4-component net radiometers (Kipp & Zonen CNR-1, Delft, Netherlands) at each of the two towers. Precipitation was measured by two tipping bucket type of rain gauges (TE-525, CSI; Onset Data Logging Rain Gauge, Onset Computer Corporation, USA).

Flux observations at 30-min time steps were quality checked, as judged by atmospheric stability and flux stationarity (Noormets et al., 2008). The 30-min data were then gap-filled using the monthly regression between observed and potential ET models created from good quality observed data. The average closure ratio for the 30-min dataset was 0.90 and 0.83 at NC1 and NC2, respectively, during daytime when net radiation is larger than 0, indicating reasonable system performance in closing the energy balance. The 30-min energy fluxes during the daytime were summed to obtain daily energy fluxes for validation.

3.3.6. Groundwater depth data

Groundwater depth data were downloaded from USGS Groundwater Watch for site number 354418076463601, located in the Washington County, NC (35° 44′N, 76° 46′ W, Fig. 1) at a depth of 4.73 m. Long-term (1986–2016) observations in this well record the lowest level being at 2.2 m below ground level, the highest level at 0.1 m with a median level at 0.74 m. The latter is within the typical taproot depth of loblolly pine (1 to 3 m), hence the need for ditch drainage within the pine plantation.

3.3.7. U.S. Drought Monitor Time series

U.S. Drought Monitor (USDM) time series data were exported from the National Drought Mitigation Center website (http://www.droughtmonitor.unl.edu/Data/Timeseries.aspx) for the 8-digit hydrologic unit code (HUC) area 03010205 (Albemarle). The dataset

[1] The use of trade, firm, or corporation names in this article is for the information and convenience of the reader. Such use does not constitute an official endorsement or approval by the United States Department of Agriculture or the Agricultural Research Service of any product or service to the exclusion of others that may be suitable.

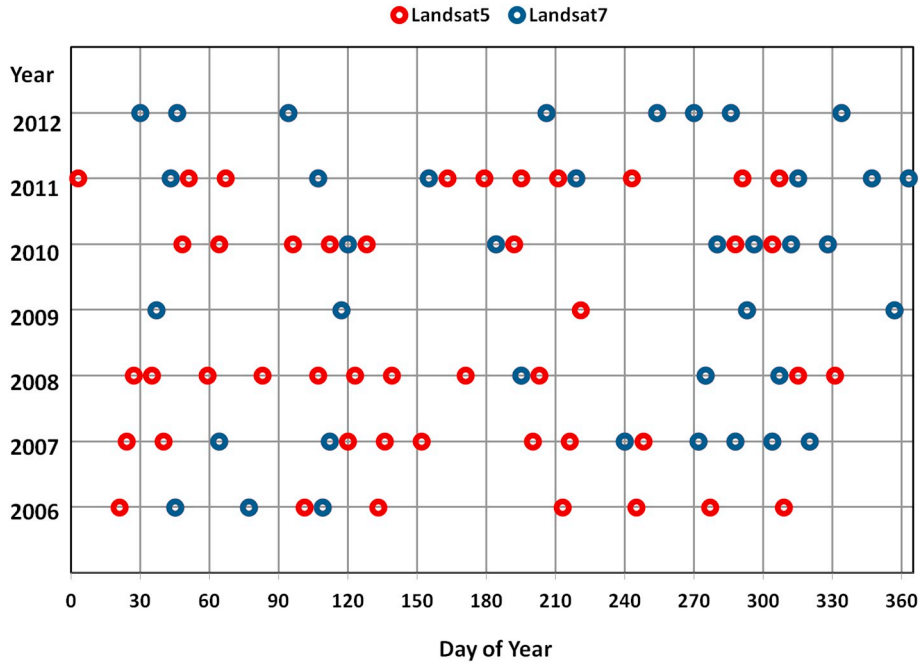

Fig. 3. Landsat overpass dates used for estimating daily evapotranspiration over the study site during 2006–2012.

characterizes percent area within this HUC area that is classified into 5 drought severity classes. D0 means there is no drought, but is experiencing abnormally dry conditions that could turn into drought or is recovering from drought. D1 indicates moderate drought, which can cause some damage to crops and pastures. D2 indicates severe drought, which can possibly cause losses of crop and pasture. D3 indicates extreme drought with major crop and pasture losses. D4 indicates exceptional drought with exceptional and widespread crop and pasture losses. In this study area, no D4 drought occurred over the study period.

4. Results

4.1. Evaluation of modeled ET at flux tower sites

To evaluate performance of the multiscale ET mapping system and the underlying TSEB energy balance model, the simulated daily ET was compared with the observations from the two flux towers, US-NC1 and US-NC2, for the period 2006 to 2012. Observed and simulated day-integrated energy flux components on Landsat dates are compared in Fig. 4, showing reasonable partitioning of the surface energy budget. The errors in modeled fluxes on Landsat dates over this 7-year period are similar to errors cited by Yang et al. (2017b) for a single year (2013) at flux towers US-NC2 and US-NC3 (the latter newly established in 2013). Solar radiation (*Rs*) and net radiation (*RN*) do not show significant bias, indicating the modeled radiative forcings are reasonable. Fig. 4 shows that daily *G* is very small and unbiased, and therefore is not contributing substantially to errors in *H* and *LE* partitioning. While the relative scatter in *H* is moderately large, the average Bowen ratio is low at these sites (~0.6) and *H* and *LE* distributions fall along the one-to-one line, demonstrating model skill in partitioning available energy among the turbulent fluxes.

Observed and simulated daily ET from the fused Landsat-MODIS time series are plotted in Fig. 5, with statistical metrics of model performance at daily and monthly timescales provided in Table 1. Generally, there was a good agreement between the observed and simulated daily ET at both sites. RMSE from 2006 to 2012 is approximately 1.1 mm d^{-1} at both sites at daily time steps and 0.5 and 0.6 mm d^{-1} at monthly time steps at NC1 and NC2 respectively, which is comparable to errors reported by Yang et al. (2017b) for this region for 2013 alone. Other fusion experiments have reported similar RMSE for daily ET estimates. For example, Cammalleri et al. reported RMSE at daily time steps of 1.1 mm d^{-1} during the growing season for rainfed and irrigated corn and soybean in central Iowa and Nebraska, and 1.5 mm d^{-1} for cotton in Bushland, Texas (Cammalleri et al., 2014). Daily 30-m ET estimates over vineyards in California exhibited an RMSE of 1.0 mm d^{-1} (Semmens et al., 2016), while Sun et al. (2017a, 2017b, 2017c) reports a lower RMSE of 0.6 mm d^{-1} for irrigated corn in the Choptank River watershed on the Eastern Shore of Maryland. Anderson et al. (2018) obtained an RMSE of 0.9 mm d^{-1} on average over multiple landcover types, including crops and wetlands, in central California.

Examining the time series behavior of modeled and measured ET in Fig. 5, we can see the model overestimated ET during the peak growing season in 2006 over NC1. This was partially due to the lack of available clear-sky Landsat imagery from April to July, such that early season fluxes were ill-constrained. The study area on the East coast of North Carolina has a high climatological level of cloud cover, and this results in a lower frequency of usable Landsat acquisitions and more gapfilling in both ALEXI and DisALEXI MODIS/Landsat than in many other parts of the United States.

4.2. Long-term trends in LAI, transpiration and cumulative ET at the flux tower sites

Fig. 6 shows the evolution of LAI extracted from the 30-m Landsat and 1-km MODIS DisALEXI input datasets at the NC1 and NC2 tower sites. In this plot, Landsat LAI is sampled on clear Landsat overpass days while MODIS LAI is interpolated to daily from the 4-day standard product. Despite the lower temporal sampling for Landsat, the behavior at both scales is reasonable and reflects both growth and management in the two pine stands. At the beginning of the simulation period (2006), the trees at NC1 and NC2 were ~4 years and ~16 years old, respectively, as reflected by the large difference in peak Landsat-scale LAI in that year. The Landsat-scale LAI at NC1 increased steadily throughout the simulation period (2006–2012), but at a somewhat slower rate in 2007 and 2008 likely due to the impact of drought. There is no obvious impact of drought on the LAI of the more mature pines at the NC2 site. Landsat-scale LAI at NC1 rapidly increased after 2009, suggesting a quick recovery from the drought. The Landsat-scale LAI at

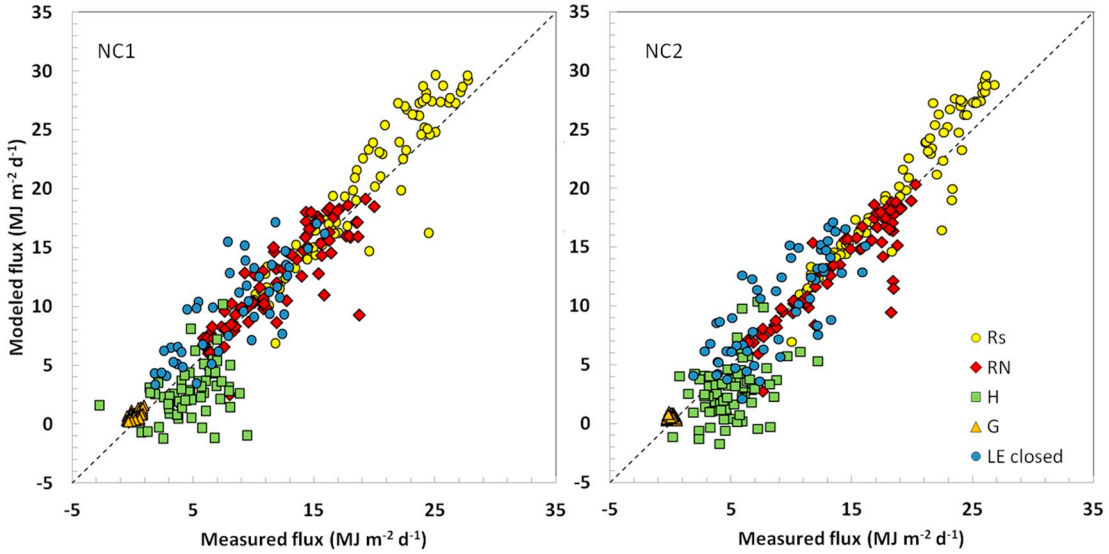

Fig. 4. Comparison between modeled and measured day-integrated energy flux components at NC1 (young plantation) and NC2 (mid-rotation) sites on clear Landsat overpass dates from 2006 to 2012. Fluxes shown include solar radiation (*Rs*), net radiation (*RN*), sensible heat (*H*), soil heat flux (*G*), and latent heat flux corrected for energy budget closure errors (*LE* closed).

NC2 dropped to its lowest value in 2010. This was a result of the thinning performed in late 2009, which most notably impacted the dormant season LAI. While Landsat-scale LAI shows variations among different years at NC1 and NC2, MODIS LAI failed to capture the change signals due to the relatively coarse spatial resolution. This demonstrates the value of Landsat-scale spatial resolution for heterogeneous land surface studies.

Canopy transpiration (T) rates estimated by the TSEB on clear Landsat overpass dates (Fig. 7) show trends similar to those in LAI (Fig. 6). At the beginning of the study period, T from the older pines at NC2 exceeds that from the NC1 site, especially during the peak growing season. The two transpiration curves converge by 2009. Drought-induced reductions in T are most notable at NC1 in 2007 and 2008, but also in 2011. The impacts of thinning in NC1 are not as apparent in the transpiration estimates as in the cold-season LAI time series. This may be because the overall radiation load and flux levels are low during the

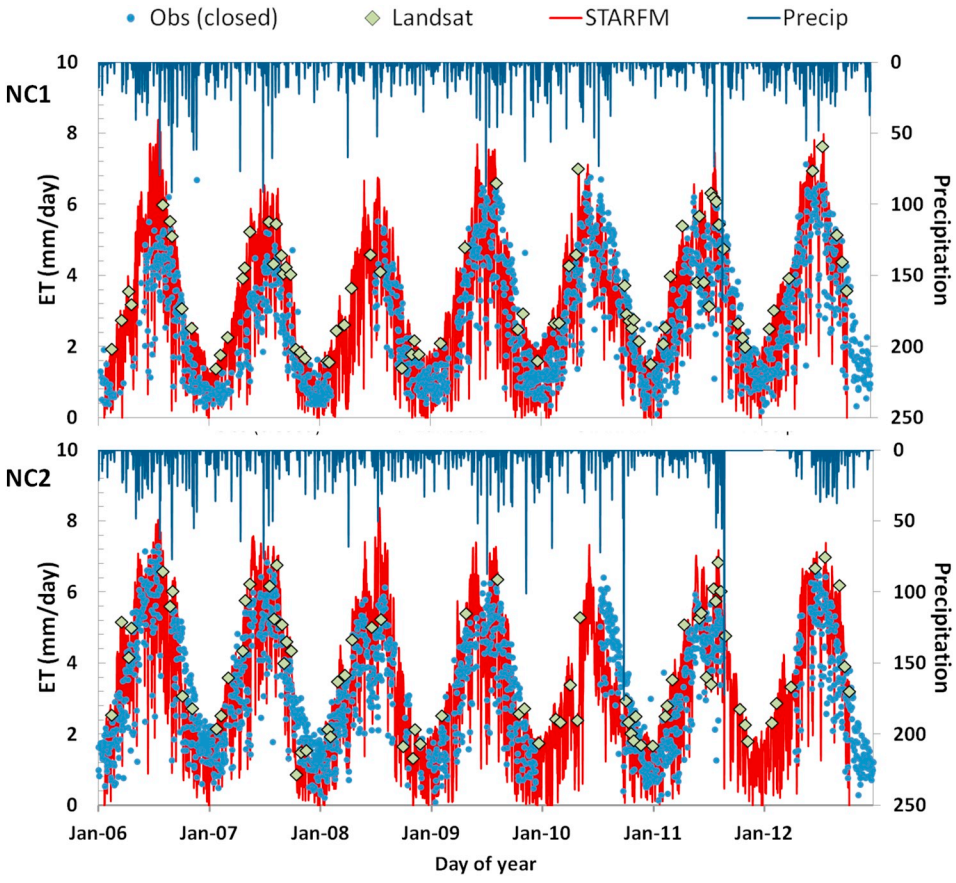

Fig. 5. Time series plot of simulated and observed 30-m daily ET at the NC1 (top, young plantation) and NC2 (below, mid-rotation plantation) site, respectively. Shown are the observed fluxes (blue circles), ET retrievals on Landsat overpass days (yellow diamonds), STARFM fused daily ET (red line) and precipitation observed at each flux tower (blue bars). There is a measurement gap at the end of 2011 and beginning of 2012 at NC2. (For interpretation of the references to color in this figure legend, the reader is referred to the web version of this article.)

Table 1
Statistical metrics[1] comparing simulated and observed 30-m daily ET at the NC1 and NC2 sites on Landsat dates and from STARFM at daily and monthly time steps.

TOWER	N	Ô	MBE	RMSE	MAE	%RE
Landsat Retrieved ET						
NC1	48	3.39	0.63	1.21	0.97	28.7
NC2	60	3.58	0.39	1.31	1.05	29.2
STARFM Daily ET						
NC1	1685	2.80	0.38	1.13	0.89	31.9
NC2	1685	3.26	0.25	1.16	0.92	28.2
STARFM Monthly ET						
NC1	78	1.98	0.38	0.50	0.27	13.4
NC2	69	2.61	0.45	0.62	0.20	7.7

[1] N is the number of observations; Ô is mean measured flux; MBE is mean bias error; RMSE is root mean square error; MAE is mean absolute error; RE is relative error, given by the mean average error (MAE) divided by the observed average ET (Ô).

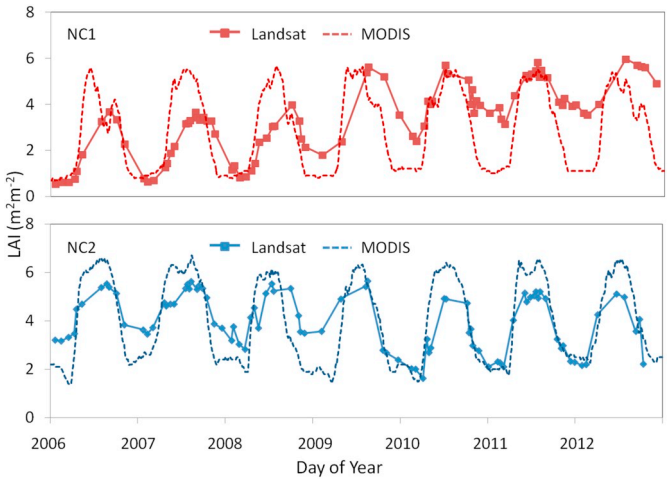

Fig. 6. LAI values extracted from Landsat and MODIS DisALEXI model inputs over the NC1 and NC2 eddy flux sites.

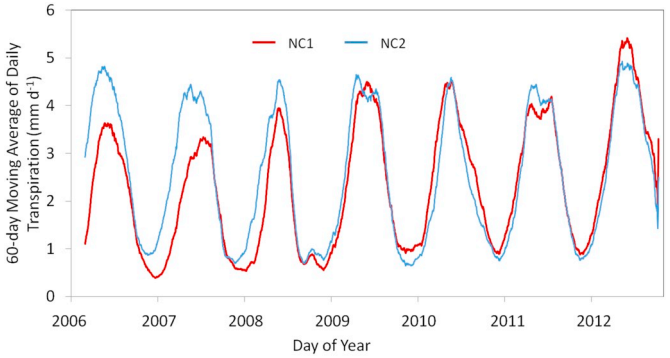

Fig. 7. Daily transpiration at NC1 and NC2 site, modeled on clear Landsat dates. These clear-sky estimates have been smoothed with a 60-day moving average to suppress noise.

cold season. However, overwinter T in NC2 is lower than in NC1 post-thinning (2009), although the signal is small.

4.3. Variations in annual ET with stand age

Understanding seasonal water use in a forested watershed, and its relationship with stand age, is important for planning effective management and anticipating impacts of stand management (e.g., clearcutting or thinning) on watershed water yield. Fig. 8 shows seasonally integrated ET computed for day of year (DOY) 50 – 330 for stands within the Weyerhaeuser pine plantation, plotted as a function of stand age. For pine stands planted after 1994 (less than ~18 years old), there is a clear linear relationship between cumulative ET and stand age, with R^2 of 0.61. This pattern is consistent with the trend reported by Yang et al., 2017b, who found a linear relationship between ET and stand age for young plantations (less than ~20 years old) using a single year of ET data. For older stands, the water use levels off and even reduces for very old stands. Of note in Fig. 8 is the response of very young plantations following the drought of 2007–2008. The red box highlights seasonal ET in 2008 and 2009 from stands planted in 2007–2009, representing the lowest rates of seasonal ET sampled and deviating from the linear portion of the curve. This suggests that the impacts of drought in this region were most felt by the very youngest stands, and lingered even after the drought was relieved in 2009.

4.4. Variations in seasonal ET and moisture stress with land cover type

Yang et al. (2017b) reported on rates of ET accumulation by different landcover types within the study area during the 2013 growing season. With a multi-year ET time series, we can extend this analysis and investigate differential impacts of variable climate on water use by landcover type. Fig. 9a shows growing season ET as a function of year for five major land cover classes and for the NC1 and NC2 flux tower sites. Here, "young plantation" represents stands that were planted during 2002–2005 (~3–10 years old over the study period) and "mature plantation" represents stands that were planted during 1985–1988 (~20–30 years old). For the NC1 and NC2 sites, average seasonal ET was extracted from a 3 by 3 pixel area centered on the tower location. Time series for the generalized landcover classes were computed from random samples extracted from the study domain based on the NLCD (n = 1000 for woody wetland and natural forest classes) and stand age map (n = 100 for plantation age classes).

ET temporal dynamics in this landscape are related in part to moisture supply from rainfall and groundwater, which are coupled in the study site during severe drought years (Fig. 9b). The climatological mean groundwater table depth (red line) ranges from 0.5 m in the spring to 1 m in fall. In response to rainfall deficits during the study period, the groundwater table depth in October of 2008 and in September of 2010 (~2 m) dropped to the lowest value since 1988. The water table returned to normal in Fall of 2011. ET dynamics, precipitation and groundwater table depth all correspond well with the USDM time series, which reports D2/D3 drought starting from the summer of 2007 and continuing to 2008. Another D2/D3 drought occurred during 2011.

Seasonal ET time series in Fig. 9 indicate differential response to drought and stand management events among the landcovers within the study domain. As in the 2013 study (Yang et al., 2017b), natural forest, woody wetland and mature plantation stands have the highest ET rates, while cropland has the lowest. Notably, modeled crop ET did not show significant impact on ET during drought in 2007 and 2008. This suggests that crop ET is primarily energy limited in this region, likely due to a combination of shallow water table and supplemental irrigation.

Small increases in seasonal ET in 2007 for both wetland and natural forest may be related to relatively higher evaporative demand during the severe drought year, enhancing evaporative losses for classes with sufficient access to water supply via shallow water table or deep rooting systems. However, in 2008, in the second year of drought, the lowest water table in 28 years (1988–2016) was measured at the USGS well site, associated with a decrease in seasonal ET for both classes. Mature plantation stands show water use behavior similar to that of natural forest, except for a marked decrease in ET in the first year of severe drought (2007). Domec et al. (2015) also reported a more rapid response to drought in managed pine stands in comparison unmanaged

Fig. 8. Seasonal ET for the years 2006–2012 (indicated by color) vs. stand age for each pine stand within the Parker Tract. The red rectangle highlights anomalously low seasonal ET for 2008 and 2009 (drought years) for new plantations established between 2007 and 2009. The black line indicates a linear regression fit for stands planted after 1994 (i.e., less than ~18 years old). (For interpretation of the references to color in this figure legend, the reader is referred to the web version of this article.)

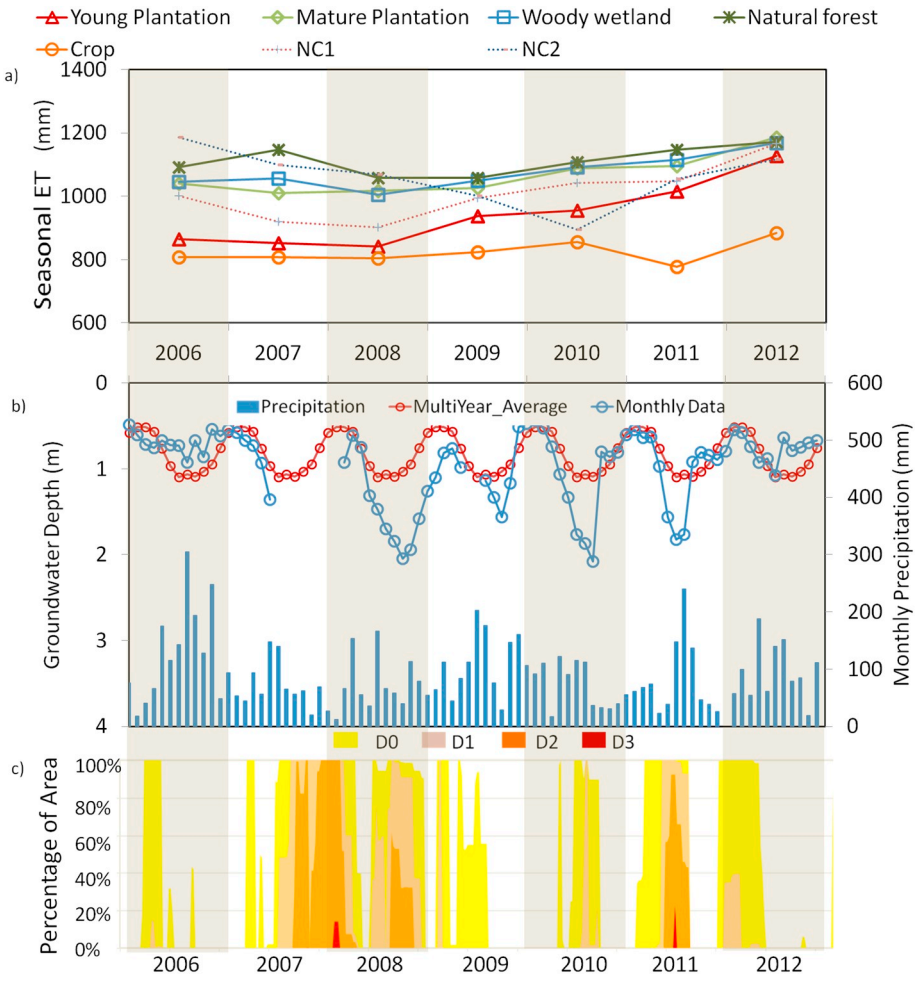

Fig. 9. a) Growing season (DOY 50-330) ET for 2006 to 2012 sampled from young and mature plantation stands within the Parker Tract, woody wetland and natural forest classes, crop, and at the NC1 and NC2 flux sites. b) Monthly precipitation from NC1 and monthly average groundwater depth. c) Time series of USDM drought classification areal percentages within the 03010205 HUC region. D0 indicates abnormally dry, D1 is moderate drought, D2 is severe drought, and D3 is extreme drought.

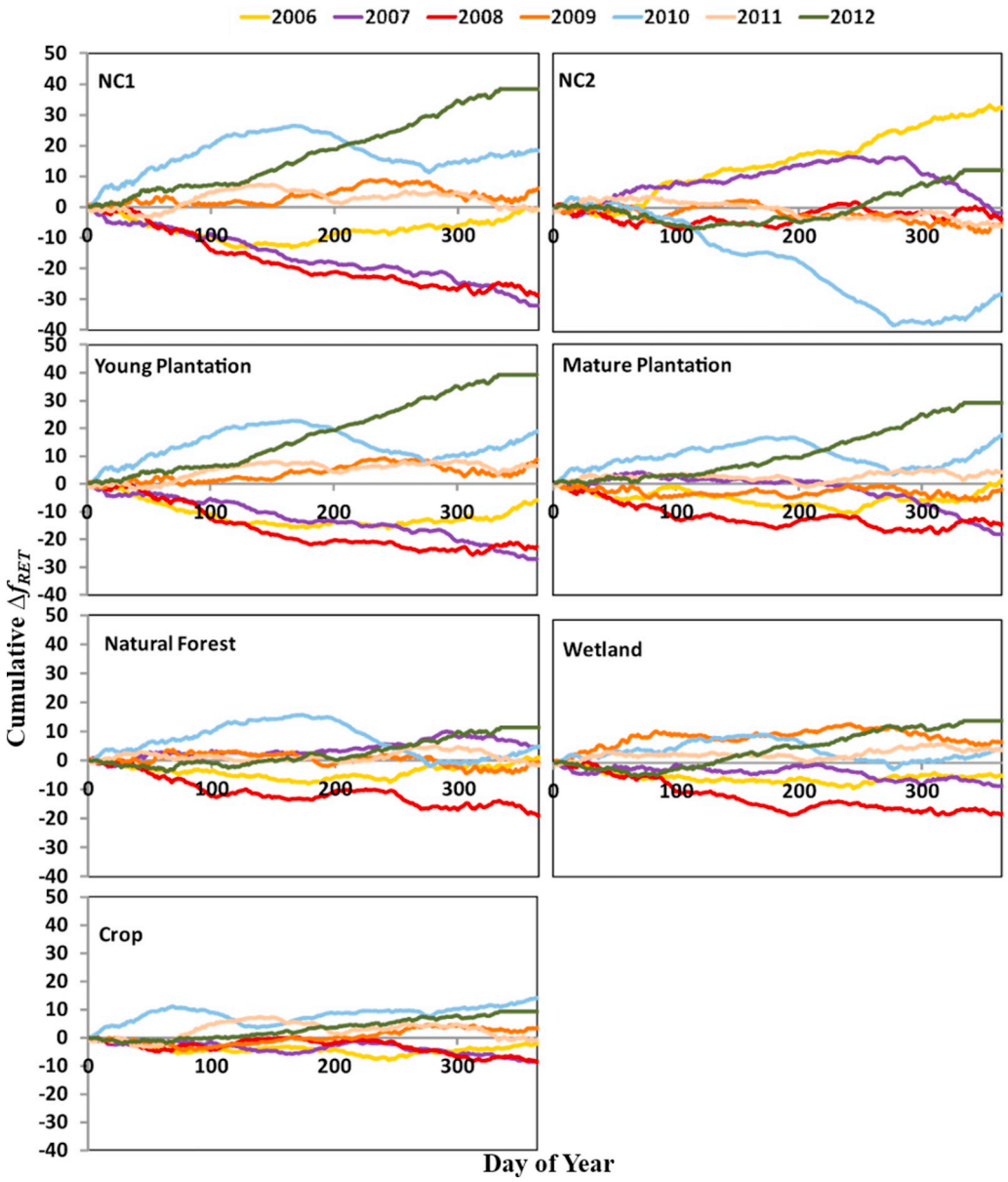

Fig. 10. Time series of cumulative Δf_{RET} for each year of the study period over NC1, NC2, natural forest, wetland, mature plantation, young plantation and cropland areas.

forest stands which demonstrates greater resilience to moisture deficits, at least over the short term. The young plantations (including NC1) show flat or decreasing ET during the extended drought of 2007–2008 – notable given the rapid annual increase in water use typical of this early growth phase (Fig. 8). This suggests enhanced drought susceptibility in young, shallow-rooted tree stands with sparse cover.

Management impacts on seasonal ET are apparent at flux site NC2. While NC1 ET evolution generally follows that of young stands in the plantation, seasonal ET at NC2 deviates strongly from that at other mature stands in 2010. This is due to the stand-specific thinning that occurred at NC2 at the end of 2009, with recovery of pre-thinning water use by the following year.

4.5. Anomalies in f_{RET} as a stress/recovery indicator

We also compared the temporal behavior of the Δf_{RET} stress metric over the study period among the five dominant land covers, as well as in the NC1 and NC2 stands, expressed as a cumulative growing season sum in Fig. 10. This cumulative metric reflects not only the changes in Δf_{RET} over the short term but also the seasonal trend of Δf_{RET}.

Generally, crop, wetland, and natural forest samples show the least interannual variability in cumulative Δf_{RET} during the study period, suggesting these classes were less impacted by drought. In cropland in this region, irrigation is employed as necessary, reducing drought sensitivity on average over the class. The deep rooting systems in natural forest and high water tables in wetlands maintain ET rates at normal levels except in 2008, the second year of an extended drought. The pine plantation sites (excluding the recent clearcut, NC1) show a gradation in drought sensitivity. The response of mature stands (planted 1985–1988) is similar to that of the natural forest class, while the young plantations (planted 2002–2005) and the NC1 site (planted 2004) show large negative deviations in cumulative Δf_{RET} in the drought years of 2007 and 2008. The anomalies in NC2 are unique due to the thinning event at the end of 2009, which drives the normal (baseline) curve to a larger extent than the drought events and leads to large negative anomalies in 2010. For all other landcover classes, high rainfall during the 2009–2010 winter alleviated dry conditions and led to large early season cumulative Δf_{RET} in 2010 until D0 drought set in mid-year.

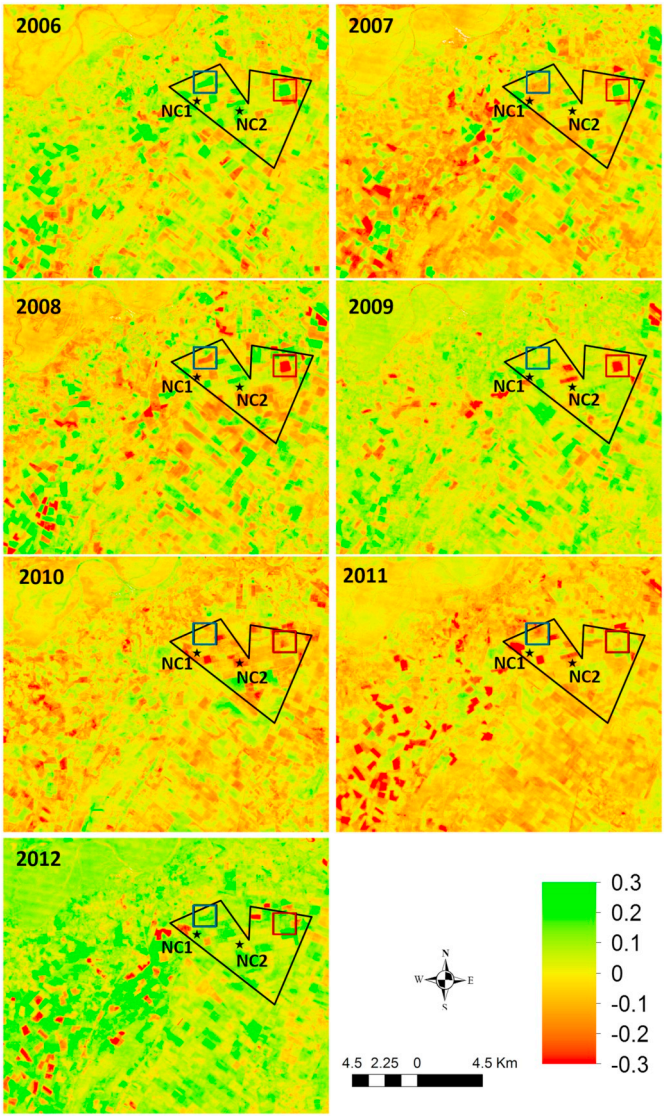

Fig. 11. Anomaly of annual average f_{RET} from 2006 to 2012. The stars represent two flux towers NC1 and NC2. The blue rectangle (site 1) highlights a field that was harvested and replanted in 2007. The red rectangle (site 2) highlights a field that was harvested at the end of 2007 and replanted in 2008. (For interpretation of the references to color in this figure legend, the reader is referred to the web version of this article.)

Maps of f_{RET} over the study area also provide useful information regarding stand response to human-induced disturbance. Fig. 11 shows maps of anomalies in annual mean f_{RET} for 2006–2012 for a subset of the full modeling domain, focusing on the Parker Tract pine plantation and neighboring agricultural lands. Time series of anomalies extracted over two disturbed stands highlighted in Fig. 11 are shown in Fig. 12. The stand in the blue box (Site 1) was harvested and replanted in 2007 and f_{RET} anomaly values show a corresponding decrease mid-year followed by a steady recovery trend over the next several years. The stand in the red box (Site 2) was harvested in 2007 and replanted in 2008, showing a similar recover trend in Fig. 12, but offset from the first time series by one year. Spatially, these recovery responses are also evident in Fig. 11.

Extracting monthly f_{RET} anomaly time series over all stands in the Parker Tract that were disturbed during the study period (identified as emerging red patches in Fig. 11), and aligning these time series on date of disturbance, we see a consistent recovery trend using simple linear trend methods (Fig. 13a). A similar trend is found in monthly NDVI

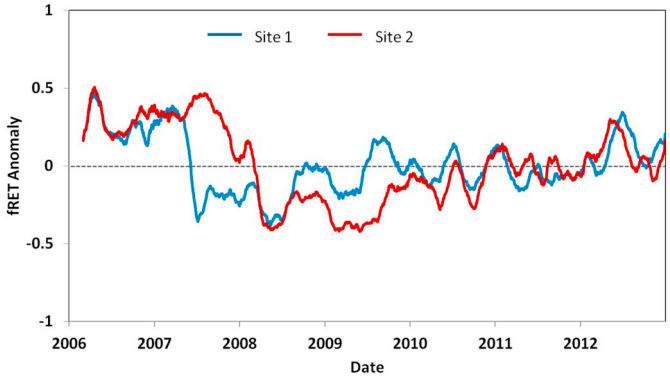

Fig. 12. Daily time series of Δf_{RET} over Site 1 and Site 2 (extracted over the polygons containing the disturbed stands located within the red and blue rectangles highlighted in Fig. 11) from 2006 to 2012. (For interpretation of the references to color in this figure legend, the reader is referred to the web version of this article.)

time series during the recovery (Fig. 13b). The NDVI observed during the growing season (indicated in red in Fig. 13b) reached a plateau earlier than the cold season NDVI (blue dots), which likely reflects index saturation at high biomass levels. The slope of the linear regression, which serves as a metric describing recovery timescale, is the same from both the f_{RET} anomaly and NDVI analyses. Since f_{RET} and NDVI are normalized as values from 0 to 1, this suggests that both indices demonstrate similar recovery trends in biomass and water use in this case.

5. Discussion

5.1. Drought impact on the study area

Although the study area is located in the humid lower coastal plain of North Carolina in a region with a shallow groundwater table, the severe drought that started in the summer of 2007 and lasted through the end of 2008 impacted annual ET of both mature and young pine stands within the managed Parker Tract plantation. In comparison with longer term precipitation trends, 2006 was a relatively wet year and can be used as a standard year to compare with drought years during the study period. The average decrease in seasonal ET from 2006 levels, computed for the major land cover classes, is 18 mm in 2007 and 65 mm in 2008, demonstrating accumulating impacts in the second year of drought. The average reduction in ET during the 2007–2008 drought from 2006 levels was about 8%. In comparison, Sun et al. estimated a 5%–10% reduction of ET within the lower coastal plain of North Carolina during the most extreme drought events that occurred in the period of 1962 to 2012 (Sun et al., 2015).

Transpiration (T) was estimated for Landsat overpass days and shows notable decreases at both flux sites within the managed pine plantation during the drought years, by approximately 27% and 11% at NC1 and NC2, respectively with respect to long-term averages (excluding the post-thinning year at NC2). Drought-induced reductions in forest transpiration were also reported in many earlier studies in different study areas (Domec et al., 2015; Limousin et al., 2009; Noormets et al., 2010; Vose and Swank, 1994; Wullschleger and Hanson, 2006). MacKay et al. studied the impact of induced drought in a temperate pine plantation forest in Southern Ontario, Canada and found 27% decrease of canopy transpiration in the drought plot at the end of the growing season (MacKay et al., 2012).

The seasonal ET and f_{RET} analyses in Figs. 10 and 11 suggest that the impact of drought on ET from young plantations is larger than that from mature stands, especially for very young seedlings. This was also reported by earlier studies. Research using observed sap-flow data in hill evergreen forest in northern Thailand found significant decrease in

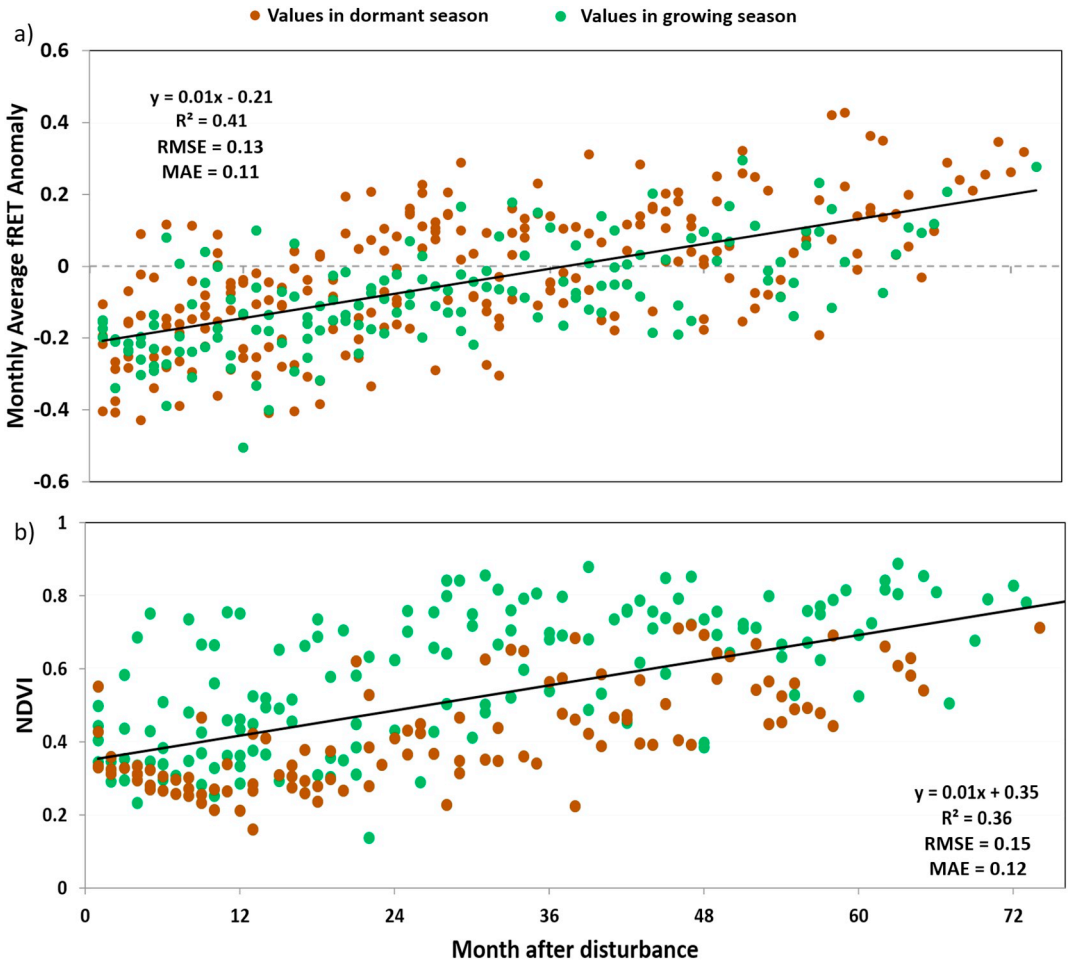

Fig. 13. a) Anomalies of monthly average f_{RET} from 2006 to 2012 for selected disturbed sites. The x-axis is the month after disturbance, identified as the time that the anomaly of monthly average f_{RET} starts to be negative. b) Plot of NDVI on Landsat overpass days for the same selected disturbed sites, aligned on date of disturbance. The brown points are data from the dormant season (November to March) and the green points are data from the growing season. Black lines indicate linear regressions for all points in each plot. (For interpretation of the references to color in this figure legend, the reader is referred to the web version of this article.)

water use in the smallest trees due to shallower roots (Kume et al., 2007). Larger trees tend to actively maintain ET during drought periods accompanied by higher levels solar radiation and VPD (Kume et al., 2007; Nepstad et al., 2004). Bennett et al. (2015) suggest that sustained high rates of ET under elevated evaporative demand might contribute to the relatively higher mortality rate of larger trees observed globally during extended droughts. In our study area, the cumulative Δf_{RET} analysis in Fig. 10 shows that ET from land cover classes returned to normal in 2009 after the 2007–2008 drought. The drought was severe but primarily affected only the growing season, which might partially contribute to the fast recovery.

During drought years, when the groundwater table depth dropped below climatologically average levels, ET from plots with seedlings and young trees was more significantly impacted than in mature stands within the pine plantation. This likely reflects the capacity of the more developed rooting systems in these mature stands to access deeper water pools. Relatively small decreases in forest ET during short-term drought in this and other regions was also discussed in other studies (Sun et al., 2010; Sun et al., 2015; Xie et al., 2014; Liu et al., 2018), and attributed to the buffering capacity of forest soils and shallow groundwater table.

5.2. Disturbance impacts and subsequent recovery in managed pine stands

Previous studies have documented that ecosystem ET is extremely variable over space and time depending on both climate and ecosystem structure (Sun et al., 2011a). Understanding seasonal water use in a forested watershed, and its relationship with stand age and disturbance, is important for planning effective management and anticipating likely effects of stand management (e.g., clearcutting or thinning) and land use change on watershed water supply (Sun and Caldwell, 2015). Forest thinning in late 2009 that aimed at improving stand productivity at the NC2 site removed about half of the basal area. LAI and ET temporally decreased due to the thinning, but recovered one year after the thinning, which might be due to rapid growth of understory vegetation. The quick recovery of understory vegetation LAI was also reported by Gavazzi et al. (2016) and Liu et al. (2018), who studied the thinning impact on canopy rainfall interception at the same study site.

Fig. 13 demonstrates the potential for integrating water use change information derived from remotely sensed ET time series into studies of land use and land cover change. For rapid onset or “flash” drought events (Otkin et al., 2017), such as the drought that rapidly enveloped the central U.S. in 2012, there is evidence that vegetation expresses a thermal stress signal before changes in optical vegetation indices like NDVI are observed (Anderson et al., 2013; Otkin et al., 2013, 2014, 2016). While the recovery trends displayed in Fig. 13 were based on manual/visual interpretation of disturbance date, change detection methods could be employed to automatically detect discontinuities in water use/stress time series for large area analyses. For example, the f_{RET} anomaly time series discussed here may be very compatible with the approach used in the Continuous Classification and Change Detection (CCDC) algorithm (Zhu et al., 2015; Zhu and Woodcock, 2014),

which detects significant breaks in reflectance band or vegetation index time series from normal annual curves. Similarly, water use change due to management practices, climate variability, insect attacks or other causality agents, and the subsequent recovery can be detected by analyzing the f_{RET} anomaly. A better of understanding water use changes resulting from land cover change will inform better management decision making in forested watersheds.

6. Conclusions

This study applied a multiscale data fusion ET model to estimate daily plot-scale ET from 2006 to 2012 over a managed forested landscape using remotely sensed data to assess the impacts of drought and disturbance on ET and the timescales of subsequent recovery to pre-disturbance levels of water use. The modeled 30-m daily ET retrievals showed good agreement with eddy covariance flux measurements made over a young plantation and a mature plantation sites, demonstrating the utility of the data fusion approach for producing reasonable ET estimates over forest stands with different levels of maturity.

In addition to total ET, the ratio of actual to reference ET, f_{RET}, and anomalies in f_{RET} appear to be useful in determining various levels of drought impact severity for different land cover types, providing a metric of resilience at the patch scale. Monthly maps of f_{RET} anomalies can be used to quantify the rate of recovery in water usage after stand disturbance. This study offers new insight to understanding the impacts of drought and disturbance on the hydrological cycle for a landscape with mixed land uses. The remote sensing methods described can provide high spatiotemporal water use information for decision making in forest management: for monitoring impacts of management such as thinning, harvesting, replanting etc. on stand water use characteristics. Future studies will apply these methods to other forested landscapes with different topographic and climatic conditions to further assess the robustness of this approach for monitoring forest water use change.

Acknowledgement

This work was funded in part by a grant from National Aeronautics and Space Administration (NNH14AX36I). We thank the Weyerhaeuser Company for providing stand age data. The U.S. Department of Agriculture (USDA) prohibits discrimination in all its programs and activities on the basis of race, color, national origin, age, disability, and where applicable, sex, marital status, familial status, parental status, religion, sexual orientation, genetic information, political beliefs, reprisal, or because all or part of an individual's income is derived from any public assistance program. (Not all prohibited bases apply to all programs.) Persons with disabilities who require alternative means for communication of program information (Braille, large print, audiotape, etc.) should contact USDA's TARGET Center at (202) 720-2600 (voice and TDD). To file a complaint of discrimination, write to USDA, Director, Office of Civil Rights, 1400 Independence Avenue, S.W., Washington, D.C. 20250-9410, or call (800) 795-3272 (voice) or (202) 720-6382 (TDD). USDA is an equal opportunity provider and employer.

References

Allen, R.G., Pereira, L.S., Raes, D., Smith, M., 1998. Crop Evapotranspiration-Guidelines for Computing Crop Water Requirements-FAO Irrigation and Drainage Paper. 56. FAO, Rome, pp. 300.

Allen, C.D., Macalady, A.K., Chenchouni, H., Bachelet, D., McDowell, N., Vennetier, M., Kitzberger, T., Rigling, A., Breshears, D.D., Hogg, E.H.T., 2010. A global overview of drought and heat-induced tree mortality reveals emerging climate change risks for forests. For. Ecol. Manag. 259, 660–684.

Anderegg, W.R.L., Kane, J.M., Anderegg, L.D.L., 2012. Consequences of widespread tree mortality triggered by drought and temperature stress. Nat. Clim. Chang. 3, 30.

Anderegg, W.R.L., Plavcová, L., Anderegg, L.D.L., Hacke, U.G., Berry, J.A., Field, C.B., 2013. Drought's legacy: multiyear hydraulic deterioration underlies widespread aspen forest die-off and portends increased future risk. Glob. Chang. Biol. 19, 1188–1196.

Anderegg, W.R., Hicke, J., Fisher, R., Allen, C., Juliann, A., Barbara, B., Sharon, H., Lichstein, J., Macalady, A., Nate, M., Yude, P., Kenneth, R., Anna, S., Shaw, J., Stephenson, N., Christina, T., Melanie, Z., 2015. Tree mortality from drought, insects, and their interactions in a changing climate. New Phytol. 208, 674–683. https://doi.org/10.1111/nph.13477.

Anderson, M.C., Norman, J.M., Diak, G.R., Kustas, W.P., Mecikalski, J.R., 1997. A two-source time-integrated model for estimating surface fluxes using thermal infrared remote sensing. Remote Sens. Environ. 60, 195–216.

Anderson, M.C., Norman, J.M., Mecikalski, J.R., Torn, R.D., Kustas, W.P., Basara, J.B., 2004. A multiscale remote sensing model for disaggregating regional fluxes to micrometeorological scales. J. Hydrometeorol. 5, 343–363.

Anderson, M.C., Norman, J.M., Kustas, W.P., Li, F., Prueger, J.H., Mecikalski, J.R., 2005. Effects of vegetation clumping on two–source model estimates of surface energy fluxes from an agricultural landscape during SMACEX. J. Hydrometeorol. 6, 892–909.

Anderson, M.C., Norman, J.M., Mecikalski, J.R., Otkin, J.A., Kustas, W.P., 2007. A climatological study of evapotranspiration and moisture stress across the continental United States based on thermal remote sensing: 1. Model formulation. J. Geophys. Res. 112, D10117. https://doi.org/10.1029/2006JD007506.

Anderson, M., Norman, J., Kustas, W., Houborg, R., Starks, P., Agam, N., 2008. A thermal-based remote sensing technique for routine mapping of land-surface carbon, water and energy fluxes from field to regional scales. Remote Sens. Environ. 112, 4227–4241. https://doi.org/10.1016/j.rse.2008.07.009.

Anderson, M.C., Kustas, W.P., Norman, J.M., Hain, C.R., Mecikalski, J.R., Schultz, L., González-Dugo, M.P., Cammalleri, C., d'Urso, G., Pimstein, A., 2010. Mapping daily evapotranspiration at field to global scales using geostationary and polar orbiting satellite imagery. Hydrol. Earth Syst. Sci. Discuss. 7, 5957–5990.

Anderson, M.C., Hain, C., Wardlow, B., Pimstein, A., Mecikalski, J.R., Kustas, W.P., 2011. Evaluation of drought indices based on thermal remote sensing of evapotranspiration over the continental United States. J. Clim. 24, 2025–2044. https://doi.org/10.1175/2010JCLI3812.1.

Anderson, M.C., Allen, R.G., Morse, A., Kustas, W.P., 2012a. Use of Landsat thermal imagery in monitoring evapotranspiration and managing water resources. Remote Sens. Environ. 122, 50–65. https://doi.org/10.1016/j.rse.2011.08.025.

Anderson, M.C., Kustas, W.P., Alfieri, J.G., Gao, F., Hain, C., Prueger, J.H., Evett, S., Colaizzi, P., Howell, T., Chávez, J.L., 2012b. Mapping daily evapotranspiration at Landsat spatial scales during the BEAREX'08 field campaign. Adv. Water Resour. 50, 162–177. https://doi.org/10.1016/j.advwatres.2012.06.005.

Anderson, M.C., Hain, C., Otkin, J., Zhan, X., Mo, K., Svoboda, M., Wardlow, B., Pimstein, A., 2013. An intercomparison of drought indicators based on thermal remote sensing and NLDAS-2 simulations with U.S. drought monitor classifications. J. Hydrometeorol. 14, 1035–1056. https://doi.org/10.1175/JHM-D-12-0140.1.

Anderson, M.C., Zolin, C.A., Sentelhas, P.C., Hain, C.R., Semmens, K., Yilmaz, M.T., Gao, F., Otkin, J.A., Tetrault, R., 2016. The Evaporative Stress Index as an indicator of agricultural drought in Brazil: an assessment based on crop yield impacts. Remote Sens. Environ. 174, 82–99.

Anderson, M., Gao, F., Knipper, K., Hain, C., Dulaney, W., Baldocchi, D., Eichelmann, E., Hemes, K., Yang, Y., Medellin-Azuara, J., 2018. Field-scale assessment of land and water use change over the California Delta using remote sensing. Remote Sens. 10.

Bailey, R., 1995. Description of the Ecoregions of the United States. USDA Forest Service, Washington.

Baldocchi, D., 1997. Measuring and modelling carbon dioxide and water vapour exchange over a temperate broad-leaved forest during the 1995 summer drought. Plant Cell Environ. 20, 1108–1122.

Bennett, A.C., McDowell, N.G., Allen, C.D., Anderson-Teixeira, K.J., 2015. Larger trees suffer most during drought in forests worldwide. Nat. Plants 1, 15139.

Boggs, J., Sun, G., McNulty, S., 2015. Effects of timber harvest on water quantity and quality in small watersheds in the Piedmont of North Carolina. J. For. 114, 27–40.

Cammalleri, C., Anderson, M.C., Gao, F., Hain, C.R., Kustas, W.P., 2013. A data fusion approach for mapping daily evapotranspiration at field scale. Water Resour. Res. 49, 4672–4686. https://doi.org/10.1002/wrcr.20349.

Cammalleri, C., Anderson, M.C., Gao, F., Hain, C.R., Kustas, W.P., 2014. Mapping daily evapotranspiration at field scales over rainfed and irrigated agricultural areas using remote sensing data fusion. Agric. For. Meteorol. 186, 1–11. https://doi.org/10.1016/j.agrformet.2013.11.001.

Clark, J.S., Iverson, L., Woodall, C.W., Allen, C.D., Bell, D.M., Bragg, D.C., D'Amato, A.W., Davis, F.W., Hersh, M.H., Ibanez, I., 2016. The impacts of increasing drought on forest dynamics, structure, and biodiversity in the United States. Glob. Chang. Biol. 22, 2329–2352.

Clinton, B.D., Elliott, K.J., Swank, W.T., 1997. Response of planted eastern white pine (*Pinus strobus* L.) to mechanical release, competition, and drought in the southern Appalachians. South. J. Appl. For. 21, 19–23.

Cohen, W.B., Yang, Z., Stehman, S.V., Schroeder, T.A., Bell, D.M., Masek, J.G., Huang, C., Meigs, G.W., 2016. Forest disturbance across the conterminous United States from 1985–2012: the emerging dominance of forest decline. For. Ecol. Manag. 360, 242–252.

Cook, M., Schott, J.R., Mandel, J., Raqueno, N., 2014. Development of an operational calibration methodology for the Landsat thermal data archive and initial testing of the atmospheric compensation component of a Land Surface Temperature (LST) product from the archive. Remote Sens. 6, 11244–11266.

Cornish, P., Vertessy, R., 2001. Forest age-induced changes in evapotranspiration and water yield in a eucalypt forest. J. Hydrol. 242, 43–63. https://doi.org/10.1016/S0022-1694(00)00384-X.

Diggs, J.A., 2004. Simulation of Nitrogen and Hydrology Loading of Forested Fields in Eastern North Carolina Using DRAINMOD-N II.

Domec, J.-C., Sun, G., Noormets, A., Gavazzi, M.J., Treasure, E.A., Cohen, E., Swenson, J.J., McNulty, S.G., King, J.S., 2012. A comparison of three methods to estimate

evapotranspiration in two contrasting loblolly pine plantations: age-related changes in water use and drought sensitivity of evapotranspiration components. For. Sci. 58, 497–512. https://doi.org/10.5849/forsci.11-051.
Domec, J.-C., King, J.S., Ward, E., Oishi, A.C., Palmroth, S., Radecki, A., Bell, D.M., Miao, G., Gavazzi, M., Johnson, D.M., 2015. Conversion of natural forests to managed forest plantations decreases tree resistance to prolonged droughts. For. Ecol. Manag. 355, 58–71.
Esper, J., Niederer, R., Bebi, P., Frank, D., 2008. Climate signal age effects—evidence from young and old trees in the Swiss Engadin. For. Ecol. Manag. 255, 3783–3789.
Fry, J., Xian, G., Jin, S., Dewitz, J., Homer, C., Yang, L., Barnes, C., Herold, N., Wickham, J., 2011. Completion of the 2006 national land cover database for the conterminous United States. PE&RS 77 (9), 858–864(Publ. by Multi-Resolution L. Charact. Consortium. Website http://www.mrlc.gov/nlcd2006.php. Accessed Oct. 24, 2013).
Gao, F., Masek, J., Schwaller, M., Hall, F., 2006. On the blending of the Landsat and MODIS surface reflectance: predicting daily Landsat surface reflectance. Geosci. Remote Sensing, IEEE Trans. 44, 2207–2218.
Gao, F., Anderson, M.C., Kustas, W.P., Wang, Y., 2012a. Simple method for retrieving leaf area index from Landsat using MODIS leaf area index products as reference. J. Appl. Remote. Sens. 6, 63551–63554.
Gao, F., Kustas, W.P., Anderson, M.C., 2012b. A data mining approach for sharpening thermal satellite imagery over land. Remote Sens. 4, 3287–3319.
Gao, F., Hilker, T., Zhu, X., Anderson, M., Masek, J., Wang, P., Yang, Y., 2015. Fusing Landsat and MODIS data for vegetation monitoring. IEEE Geosci. Remote Sens. Mag. 3, 47–60.
Gao, F., Anderson, M.C., Zhang, X., Yang, Z., Alfieri, J.G., Kustas, W.P., Mueller, R., Johnson, D.M., Prueger, J.H., 2017. Toward mapping crop progress at field scales through fusion of Landsat and MODIS imagery. Remote Sens. Environ. 188, 9–25.
Gavazzi, M.J., Sun, G., McNulty, S.G., Treasure, E.A., Wightman, M.G., 2016. Canopy rainfall interception measured over ten years in a coastal plain loblolly pine (*Pinus taeda* L.) plantation. Trans. ASABE 59 (2), 601–610. https://doi.org/10.13031/trans.59.11101.
Huang, C., Goward, S.N., Masek, J.G., Thomas, N., Zhu, Z., Vogelmann, J.E., 2010. An automated approach for reconstructing recent forest disturbance history using dense Landsat time series stacks. Remote Sens. Environ. 114, 183–198.
Karnieli, A., Agam, N., Pinker, R.T., Anderson, M., Imhoff, M.L., Gutman, G.G., Panov, N., Goldberg, A., 2010. Use of NDVI and land surface temperature for drought assessment: merits and limitations. J. Clim. 23, 618–633. https://doi.org/10.1175/2009jcli2900.1.
Kennedy, R.E., Andréfouët, S., Cohen, W.B., Gómez, C., Griffiths, P., Hais, M., Healey, S.P., Helmer, E.H., Hostert, P., Lyons, M.B., 2014. Bringing an ecological view of change to Landsat-based remote sensing. Front. Ecol. Environ. 12, 339–346.
Kume, T., Takizawa, H., Yoshifuji, N., Tanaka, K., Tantasirin, C., Tanaka, N., Suzuki, M., 2007. Impact of soil drought on sap flow and water status of evergreen trees in a tropical monsoon forest in northern Thailand. For. Ecol. Manag. 238, 220–230.
Kustas, W., Anderson, M., 2009. Advances in thermal infrared remote sensing for land surface modeling. Agric. For. Meteorol. 149, 2071–2081. https://doi.org/10.1016/j.agrformet.2009.05.016.
Kustas, W.P., Norman, J.M., 1996. A Two-source Energy Balance Approach Using Directional Radiometric Temperature Observations for Sparse Canopy Covered Surfaces.
Kustas, W.P., Norman, J.M., 1999. Evaluation of soil and vegetation heat flux predictions using a simple two-source model with radiometric temperatures for partial canopy cover. Agric. For. Meteorol. 94, 13–29.
Kustas, W.P., Norman, J.M., 2000. A two-source energy balance approach using directional radiometric temperature observations for sparse canopy covered surfaces. Agron. J. 92, 847–854.
Limousin, J.M., Rambal, S., Ourcival, J.M., Rocheteau, A., Joffre, R., Rodríguez-Cortina, R., 2009. Long-term transpiration change with rainfall decline in a Mediterranean Quercus ilex forest. Glob. Chang. Biol. 15, 2163–2175.
Liu, X., Sun, G., Mitra, B., Noormets, A., Gavazzi, M.J., Domec, J.-C., Hallema, D.W., Li, J., Fang, Y., King, J.S., 2018. Drought and thinning have limited impacts on evapotranspiration in a managed pine plantation on the southeastern United States coastal plain. Agric. For. Meteorol. 262, 14–23.
MacKay, S.L., Arain, M.A., Khomik, M., Brodeur, J.J., Schumacher, J., Hartmann, H., Peichl, M., 2012. The impact of induced drought on transpiration and growth in a temperate pine plantation forest. Hydrol. Process. 26, 1779–1791.
Masek, J.G., Huang, C., Wolfe, R., Cohen, W., Hall, F., Kutler, J., Nelson, P., 2008. North American forest disturbance mapped from a decadal Landsat record. Remote Sens. Environ. 112, 2914–2926.
Myneni, R.B., Hoffman, S., Knyazikhin, Y., Privette, J.L., Glassy, J., Tian, Y., Wang, Y., Song, X., Zhang, Y., Smith, G.R., Lotsch, A., Friedl, M., Morisette, J.T., Votava, P., Nemani, R.R., Running, S.W., 2002. Global products of vegetation leaf area and fraction absorbed PAR from year one of MODIS data. Remote Sens. Environ. 83, 214–231. Pii S0034-4257(02)00074-3. https://doi.org/10.1016/S0034-4257(02)00074-3.
Nepstad, D., Lefebvre, P., Lopes da Silva, U., Tomasella, J., Schlesinger, P., Solorzano, L., Moutinho, P., Ray, D., Guerreira Benito, J., 2004. Amazon drought and its implications for forest flammability and tree growth: a basin-wide analysis. Glob. Chang. Biol. 10, 704–717. https://doi.org/10.1111/j.1529-8817.2003.00772.x.
Noormets, A., McNulty, S.G., DeForest, J.L., Sun, G., Li, Q., Chen, J., 2008. Drought during canopy development has lasting effect on annual carbon balance in a deciduous temperate forest. New Phytol. 179, 818–828.
Noormets, A., Gavazzi, M.J., Mcnulty, S.G., Domec, J.C., Sun, G., King, J.S., Chen, J., 2010. Response of carbon fluxes to drought in a coastal plain loblolly pine forest. Glob. Chang. Biol. 16, 272–287. https://doi.org/10.1111/j.1365-2486.2009.01928.x.
Norman, J.M., Kustas, W.P., Humes, K.S., 1995. Source approach for estimating soil and vegetation energy fluxes in observations of directional radiometric surface temperature. Agric. For. Meteorol. 77, 263–293. https://doi.org/10.1016/0168-1923(95)02265-Y.
Norman, J.M., Anderson, M.C., Kustas, W.P., French, A.N., Mecikalski, J., Torn, R., Diak, G.R., Schmugge, T.J., Tanner, B.C.W., 2003. Remote sensing of surface energy fluxes at 101-m pixel resolutions. Water Resour. Res. 39https://doi.org/10.1029/2002WR001775. n/a-n/a.
Oishi, A.C., Oren, R., Stoy, P.C., 2008. Estimating components of forest evapotranspiration: a footprint approach for scaling sap flux measurements. Agric. For. Meteorol. 148, 1719–1732. https://doi.org/10.1016/J.AGRFORMET.2008.06.013.
Otkin, J.A., Anderson, M.C., Hain, C., Mladenova, I.E., Basara, J.B., Svoboda, M., 2013. Examining rapid onset drought development using the thermal infrared–based evaporative stress index. J. Hydrometeorol. 14, 1057–1074. https://doi.org/10.1175/JHM-D-12-0144.1.
Otkin, J.A., Anderson, M.C., Hain, C., Svoboda, M., 2014. Examining the relationship between drought development and rapid changes in the evaporative stress index. J. Hydrometeorol. 15, 938–956. https://doi.org/10.1175/JHM-D-13-0110.1.
Otkin, J.A., Anderson, M.C., Hain, C., Svoboda, M., Johnson, D., Mueller, R., Tadesse, T., Wardlow, B., Brown, J., 2016. Assessing the evolution of soil moisture and vegetation conditions during the 2012 United States flash drought. Agric. For. Meteorol. 218, 230–242.
Otkin, J., Svoboda, M., Hunt, E., Anderson, M., Hain, C.R., Basara, J., 2017. Flash droughts: a review and assessment of the challenges imposed by rapid onset droughts in the United States. Bull. Am. Meteorol. Soc. https://doi.org/10.1175/BAMS-D-17-0149.1.
Saha, S., Moorthi, S., Pan, H.L., Wu, X., Wang, J., Nadiga, S., Tripp, P., Kistler, R., Woollen, J., Behringer, D., 2010. The NCEP climate forecast system reanalysis. Bull. Am. Meteorol. Soc. 91, 1015.
Saleska, S.R., Didan, K., Huete, A.R., Da Rocha, H.R., 2007. Amazon forests green-up during 2005 drought. Science (80-.) 318, 612.
Sandholt, I., Rasmussen, L., Andersen, J., 2002. A simple interpretation of TS_NDVI space for assessment of surface moisture status. Remote Sens. Environ. 79, 213–224.
Semmens, K.A., Anderson, M.C., Kustas, W.P., Gao, F., Alfieri, J.G., McKee, L., Prueger, J.H., Hain, C.R., Cammalleri, C., Yang, Y., 2016. Monitoring daily evapotranspiration over two California vineyards using Landsat 8 in a multi-sensor data fusion approach. Remote Sens. Environ. 185, 155–170.
Sims, D.A., Rahman, A.F., Cordova, V.D., El-Masri, B.Z., Baldocchi, D.D., Flanagan, L.B., Goldstein, A.H., Hollinger, D.Y., Misson, L., Monson, R.K., 2006. On the use of MODIS EVI to assess gross primary productivity of North American ecosystems. J. Geophys. Res. Biogeosci. 111.
Sun, G., Caldwell, P., 2015. Impacts of urbanization on stream water quantity and quality in the US. Water Resour. Impact 17, 17–20.
Sun, G., Noormets, A., Gavazzi, M.J., McNulty, S.G., Chen, J., Domec, J.C., King, J.S., Amatya, D.M., Skaggs, R.W., 2010. Energy and water balance of two contrasting loblolly pine plantations on the lower coastal plain of North Carolina, USA. For. Ecol. Manag. 259, 1299–1310.
Sun, G., Alstad, K., Chen, J., Chen, S., Ford, C.R., Lin, G., Liu, C., Lu, N., Mcnulty, S.G., Miao, H., Noormets, A., Vose, J.M., Wilske, B., Zeppel, M., Zhang, Y., 2011a. A General Predictive Model for Estimating Monthly Ecosystem Evapotranspiration. 255. pp. 245–255. https://doi.org/10.1002/eco.
Sun, G., Caldwell, P., Noormets, A., McNulty, S.G., Cohen, E., Moore Myers, J., Domec, J.C., Treasure, E., Mu, Q., Xiao, J., John, R., Chen, J., 2011b. Upscaling key ecosystem functions across the conterminous United States by a water-centric ecosystem model. J. Geophys. Res. 116, G00J05. https://doi.org/10.1029/2010JG001573.
Sun, S., Sun, G., Caldwell, P., McNulty, S., Cohen, E., Xiao, J., Zhang, Y., 2015. Drought impacts on ecosystem functions of the U.S. National Forests and Grasslands: part II assessment results and management implications. For. Ecol. Manag. https://doi.org/10.1016/j.foreco.2015.04.002.
Sun, G., Domec, J., Amatya, D.M., 2016. Forest evapotranspiration: measurement and modelling at multiple scales. In: Forest Hydrology: Processes, Management and Assessment, pp. 32–50. https://doi.org/10.1079/9781780646602.0000.
Sun, L., Anderson, M.C., Gao, F., Hain, C., Alfieri, J.G., Sharifi, A., McCarty, G.W., Yang, Y., Yang, Y., Kustas, W.P., 2017a. Investigating water use over the Choptank River Watershed using a multisatellite data fusion approach. Water Resour. Res. https://doi.org/10.1002/2017WR020700.
Sun, G., Hallema, D., Asbjornsen, H., 2017b. Ecohydrological processes and ecosystem services in the Anthropocene: a review. Ecol. Process. 6, 35.
Sun, Q., Wang, Z., Li, Z., Erb, A., Schaaf, C.B., 2017c. Evaluation of the global MODIS 30 arc-second spatially and temporally complete snow-free land surface albedo and reflectance anisotropy dataset. Int. J. Appl. Earth Obs. Geoinf. 58, 36–49. https://doi.org/10.1016/j.jag.2017.01.011.
Verbesselt, J., Robinson, A., Stone, C., Culvenor, D., 2009. Forecasting tree mortality using change metrics derived from MODIS satellite data. For. Ecol. Manag. 258, 1166–1173.
Vose, J.M., Swank, W.T., 1994. Effects of long-term drought on the hydrology and growth of a white pine plantation in the southern Appalachians. For. Ecol. Manag. 64, 25–39.
Wan, Z., Zhang, Y., Zhang, Q., Li, Z.L., 2004. Quality assessment and validation of the MODIS global land surface temperature. Int. J. Remote Sens. 25, 261–274.
Wang, Z., Erb, A.M., Schaaf, C.B., Sun, Q., Liu, Y., Yang, Y., Shuai, Y., Casey, K.A., Román, M.O., 2016. Early spring post-fire snow albedo dynamics in high latitude boreal forests using Landsat-8 OLI data. Remote Sens. Environ. 185, 71–83. https://doi.org/10.1016/j.rse.2016.02.059.
Wulder, M.A., White, J.C., Goward, S.N., Masek, J.G., Irons, J.R., Herold, M., Cohen, W.B., Loveland, T.R., Woodcock, C.E., 2008. Landsat continuity: issues and opportunities for land cover monitoring. Remote Sens. Environ. 112, 955–969.

Wullschleger, S.D., Hanson, P.J., 2006. Sensitivity of canopy transpiration to altered precipitation in an upland oak forest: evidence from a long-term field manipulation study. Glob. Chang. Biol. 12, 97–109.

Xie, J., Sun, G., Chu, H., Liu, J., McNulty, S.G., Noormets, A., John, R., Ouyang, Z., Zha, T., Li, H., 2014. Long-term variability in the water budget and its controls in an oak-dominated temperate forest. Hydrol. Process. 28, 6054–6066.

Yang, Y., Anderson, M., Gao, F., Hain, C., Kustas, W., Meyers, T., Crow, W., Finocchiaro, R., Otkin, J., Sun, L., 2017a. Impact of tile drainage on evapotranspiration in South Dakota, USA, based on high spatiotemporal resolution evapotranspiration time series from a multisatellite data fusion system. IEEE J. Sel. Top. Appl. Earth Obs. Remote Sens. 10, 2550–2564. https://doi.org/10.1109/JSTARS.2017.2680411.

Yang, Y., Anderson, M.C., Gao, F., Hain, C.R., Semmens, K.A., Kustas, W.P., Noormets, A., Wynne, R.H., Thomas, V.A., Sun, G., 2017b. Daily Landsat-scale evapotranspiration estimation over a forested landscape in North Carolina, USA using multi-satellite data fusion. Hydrol. Earth Syst. Sci. 21, 1017–1037. https://doi.org/10.5194/hess-21-1017-2017.

Yang, Y., Anderson, M.C., Gao, F., Wardlow, B., Hain, C.R., Otkin, J.A., Alfieri, J., Yang, Y., Sun, L., Dulaney, W., 2018. Field-scale mapping of evaporative stress indicators of crop yield: an application over Mead, NE, USA. Remote Sens. Environ. 210, 387–402.

Zhu, Z., 2017. Change detection using landsat time series: a review of frequencies, preprocessing, algorithms, and applications. ISPRS J. Photogramm. Remote Sens. 130, 370–384. https://doi.org/10.1016/j.isprsjprs.2017.06.013.

Zhu, Z., Woodcock, C.E., 2014. Continuous change detection and classification of land cover using all available Landsat data. Remote Sens. Environ. 144, 152–171. https://doi.org/10.1016/j.rse.2014.01.011.

Zhu, Z., Woodcock, C.E., Olofsson, P., 2012. Continuous monitoring of forest disturbance using all available Landsat imagery. Remote Sens. Environ. 122, 75–91.

Zhu, Z., Woodcock, C.E., Holden, C., Yang, Z., 2015. Generating synthetic Landsat images based on all available Landsat data: predicting Landsat surface reflectance at any given time. Remote Sens. Environ. 162, 67–83. https://doi.org/10.1016/j.rse.2015.02.009.